Korean J. Chem. Eng., 37(9), 1623-1630 (2020)
DOI: 10.1007/s11814-020-0550-1

pISSN: 0256-1115
eISSN: 1975-7220

Filler size effect in graphite/paraffine wax composite on electromagnetic interference shielding performance

Sosan Hwang, Chae Lin Kim, Yongha Kim, Min Gyu Song, Jaewon Lee, Sung-Hyeon Baeck, Sang Eun Shim†, and Yingjie Qian†

Department of Chemical Engineering, Inha University, 100 Inha-ro, Michuhol-gu, Incheon 22212, Korea
(*Received 13 November 2019 • Revised 29 February 2020 • Accepted 24 March 2020*)

Abstract−Graphite exhibits electromagnetic wave attenuation and high electrical conductivity. In this study, we analyzed the electromagnetic interference shielding effectiveness (EMI SE) performance and electric conductivity of composites fabricated by varying the size (mean size: 6-100 μm) of graphite fillers and explained resulting attributes through the relative permittivity and geometrical characteristics of the filler. When the graphite/paraffine wax composite was fabricated using large-sized graphite (KS150), the spacing between the graphite fillers became widened, enabling electromagnetic waves to leak through the gap. The analysis results indicated that KS150 graphite exhibited an EMI SE performance of under 10 dB when the filler content was 30 wt%. However, when the content was increased to 50 wt%, the EMI SE performance improved sharply to 40 dB. In contrast, when the composite was filled with small-sized graphite (KS6), having a high ratio of surface to volume, the EMI SE performance was greater than that with the large-sized graphite at low loading. The results related to the EMI shielding performance of graphite-filled composites revealed that the size of the filler greatly affects the EMI SE. The composite using KS75 showed an EMI SE performance of 53.0 dB and electrical conductivity of 2,000 S/m.

Keywords: Graphite, Electromagnetic Interference Shielding, Electrical Conductivity, Relative Permittivity, Geometrical Characteristics

INTRODUCTION

With the onset of the 5G communication era, the extensive utilization of electronic devices and communication facilities in civil and industrial affairs, as well as aeronautics, provides the public with better experience and convenience. However, with the rapid development of modern technology, electromagnetic interference (EMI) pollution, which not only affects the operation of electronic devices but also potentially harms biological systems, is considered one of the most significant issues threatening human safety. Therefore, it is important to develop EMI shielding materials that have been recently attracting significant interests [1-3].

Over the past decade, significant attention has been paid to the development of EMI shielding materials with high efficiency and wide shielding frequency. Generally, EMI shielding is achieved by conducting polymer composites that comprise insulating polymers and conductive fillers such as metals and carbon-based materials [4]. One kind of conductive material, metals, can shield electromagnetic waves. Regardless of the external electric field, if no current flows, the electric field inside the metal is zero, and when the surface of the metal is placed in the electric field, the free charge is internally aligned to offset the external electric field. For this reason, metals and alloys can cancel electromagnetic waves rather than attenuate the electromagnetic waves [5-7]. However, metal and alloys, which are the most conventional materials used for EMI shielding, suffer from easy-corrosion, high weight density, poor scratch resistance, and processing difficulty [8-11]. Meanwhile, the interest in conducting carbon-based fillers has been particularly elevated due to the difficulties in resolving the inherent problems of metal-based fillers as well as the demands for advanced EMI attenuating materials. Carbon materials are expected to exhibit high-performance EM wave attenuation due to their thermally activated carrier hopping associated with defect states [12-18]. Recently, several carbon-based materials such as carbon nanotube (CNT), carbon nanofiber (CNF), and graphene have been reported as alternatives for EMI shielding additives owing to their corrosion resistance and low density. Li et al. fabricated a reduced graphene oxide (rGO)/polystyrene segregated composite having EMI shielding effectiveness (EMI SE) of 45 dB at only 3.47 vol% [19]. Wei et al. prepared a multifunctional material (CNT-graphene) that exhibits ultrahigh EMI shielding performance of an EMI SE of 47.5 dB in X-band at 1.6 mm where CNT-graphene as a filler was synthesized via template-directed chemical vapor deposition [20]. A flexible Fe_3O_4/rGO-filled composite prepared by Xia et al. exhibited an EMI SE of 26.4 dB and maintained an excellent performance even after 2000 bending-release cycles [21]. A natural rubber composite filled with 10.0 wt% CNT displayed an EMI SE of 59.8 dB in X-band at 2.6 mm, and a composite filled with 5.0 wt% CNT in rubber had EMI SE of 39.2 dB even after stretching, bending, twisting [22]. Verma et al. demonstrated that a polyurethane composite filled with 7.0 wt% GNS (Graphene nano-sheets) exhibited EMI SE of 21 dB (X-band, 3.0 mm) [23]. Yang et al. fabricated an LLDPE composite filled

†To whom correspondence should be addressed.
E-mail: yjqian@inha.ac.kr, seshim@inha.ac.kr
Copyright by The Korean Institute of Chemical Engineers.

with 31.6 vol% expanded graphite showing EMI SE of 44.8 dB in X-band at 1.5 mm [24]. Appropriately, most earlier studies have reported specific skills and/or complicated processes required for regulating the EMI shielding performance. However, from a practical point of view, developing affordable and easily accessible EMI shielding materials using simple procedures can be a significant breakthrough. Compared to other carbon-based materials, currently graphite is of high interest owing to its cost-effectiveness and abundant availability as well as its superior electrical, thermal, and mechanical properties. Bellis et al. reported that graphite nanoplatelets, having a high cross-section area and aspect ratio, increased not only the dielectric loss but also the electrical loss and illustrated the possibility of a single filler possessing two electromagnetic properties [25]. Generally, the real part of effective permittivity (ε'), which is the representative of the polarizability of a material, increases with an increase in the loading of fillers with a low aspect ratio such as graphite and graphene [25]. On the contrary, the imaginary part of effective permittivity (ε''), which is related to the attenuating rate of a material, is directly proportional to the loading of materials with a high aspect ratio such as CNT and CNF [12-18].

Therefore, a comprehensive study regarding the characterizations over the X and Ku frequency (8-18 GHz) of complex permittivity of composites filled with graphite is of paramount importance. Even though some experimental results related to the morphology of graphite and EMI SE over a wide radio frequency exist, the general correlation between the graphite filler and these features is not completely defined [26]. The purpose of the current work was to investigate whether the use of affordable and abundant graphite as a single filler enables the EMI shielding composites to exhibit an enhanced EMI shielding performance. Thus, we fabricated the graphite/paraffin composites, in which paraffin was considered as the polymer matrix due to its limited influence on EMI shielding performances. We explored the size effect of graphite on EMI shielding performance by varying the size and loading amount of graphite fillers and discovered that these two factors significantly affect the EMI shielding performance. The degree of dispersion of graphite in composites was identified using micro-CT (computed tomography). Additionally, the electrical conductivity of the composite was measured to validate the correlation between the relative permittivity and the electrical conductivity [27,28].

EXPERIMENTAL

1. Materials

Synthetic graphites with four different sizes were supplied by Timcal Graphite & Carbon (Switzerland): KS6, KS44, KS75, and KS150. The paraffin (mp. ≥65 °C) wax was purchased from Sigma-Aldrich (USA). *N*-hexane was supplied by Daejung Chemicals & Metals Co., Ltd. (≥95%, S. Korea) to assist in mixing and dispersing.

2. Fabrication of Graphite-filled Composites

Four different types of graphite were mixed with paraffin wax at four different loadings (30-60 wt%) to form 12 composites using a facile method. The sample code is named G (graphite grade)-graphite content. For example, the G44-30 suspension was prepared by mixing 0.6 g of KS44 graphite, 1.4 g of paraffin wax, and 5.0 g of n-haxane; then, the suspension was stirred at 60 °C for 60 min. The G44-30 composite was obtained by removing n-hexane at 80 °C. The G44-30 composite was pressed into a toroid with an outer diameter of 7.0 mm, an inner diameter of 3.0 mm, and a height of 2.0 mm. The toroid-shaped composite was obtained at a constant force of 1,400 N using an auto press at 68 °C.

3. Characterization

To observe the surface characteristics of graphite, a field emission scanning electron microscope (SEM, Hitachi, S-4300SE, Japan) was used, and laser particle size analyzer (PSA, Malvern Instruments, Mastersizer 2000, UK) was used to confirm the size distribution of graphite. The complex permittivity value was obtained by measuring the S_{11} and S_{21} parameters over 8.0-18.0 GHz using a vector network analyzer (VNA, Anritsu, MS46122B, Japan). The dimensions of specimens and experimental setup for measuring S parameters are depicted in Scheme 1. Micro CT analysis was performed for the composites with 2 mm thickness for determining geometric characteristics of graphite in a matrix (Micro-CT, Skyscan, Skyscan-1172TM, Belgium). The electrical conductivity was measured with a 0.5 mm thick composite (Mitsubishi, Loresta-GX MCP-T700, Japan).

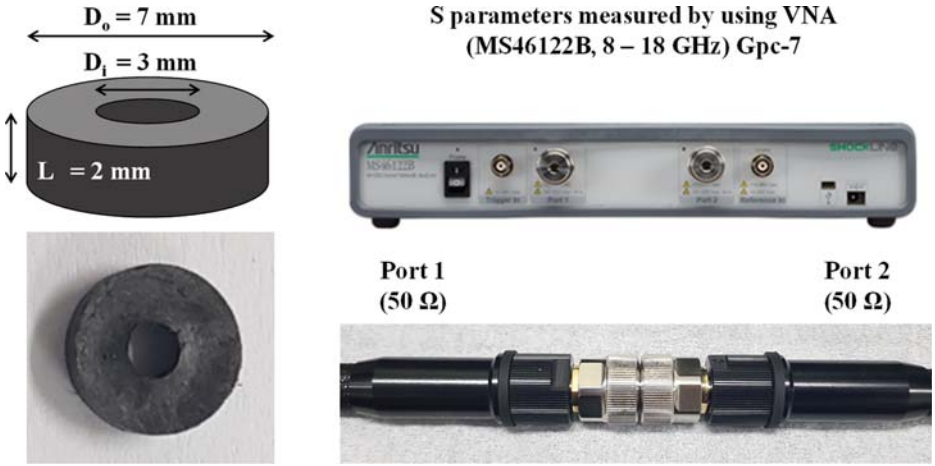

Scheme 1. The appearance of specimen used with experimental instrument for S-parameter measurement.

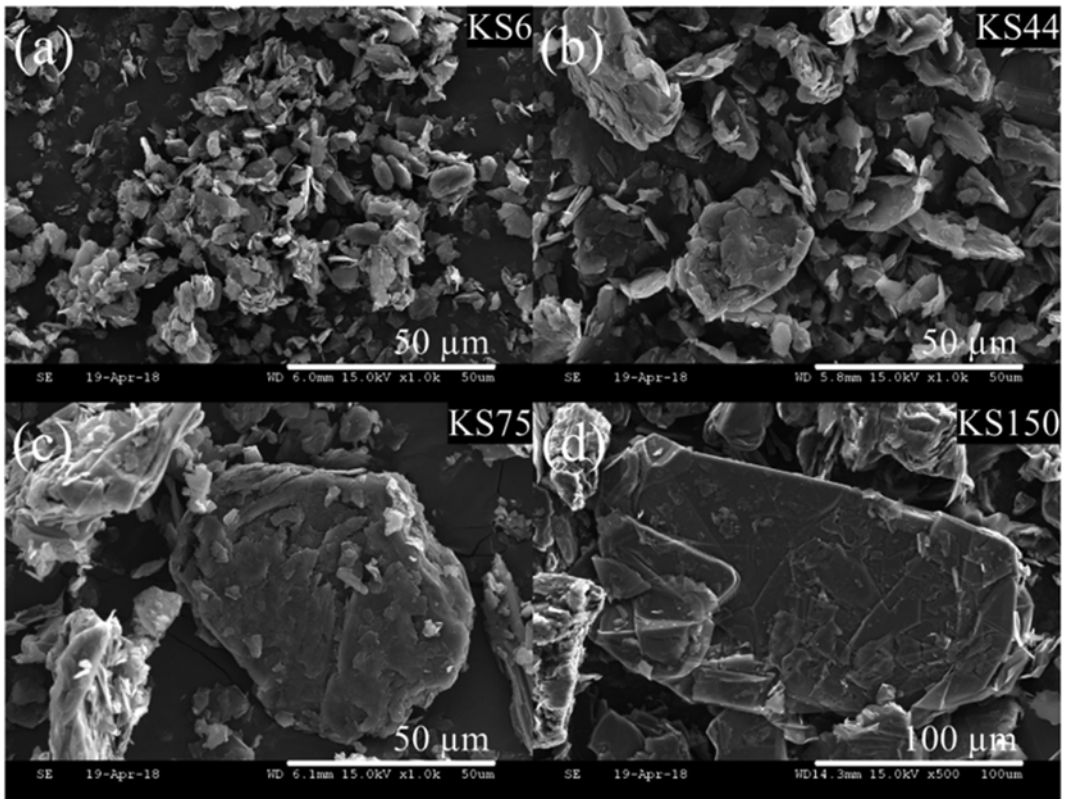

Fig. 1. SEM images of graphite: (a) KS6, (b) KS44, (c) KS75 and (d) KS150.

RESULTS AND DISCUSSION

The EM wave attenuation of composites containing carbon fillers depends on the dispersion degree of the fillers within the composites. The dispersion of fillers also affects the electrical conductivity and thermal conductivity [29]. Fig. 1 shows the scanning electron microscopy (SEM) microphotographs of graphite. All four types of graphite exhibited a similar morphology but different mean sizes. This enabled us to specifically investigate the effect of the size on the dispersibility of the filler in a matrix, which aids in determining the EMI SE performance. Usually, the size of the graphite and spacing between the graphite affect the performance.

The size distribution of graphite was analyzed using a PSA as demonstrated in Fig. 2. From this analysis, the actual sizes of graphite are identified as follows: KS6 (d_{10}: 2.030 μm, d_{50}: 5.301 μm, d_{90}: 11.189 μm), KS44 (d_{10}: 4.304 μm, d_{50}: 15.327 μm, d_{90}: 31.283 μm), KS75 (d_{10}: 5.940 μm, d_{50}: 21.414 μm, d_{90}: 55.729 μm), and KS150 (d_{10}: 10.206 μm, d_{50}: 40.883 μm, d_{90}: 111.680 μm).

After the fabrication of the composites by mixing paraffin wax and graphite, the micro-CT analysis was conducted to investigate the dispersibility of fillers in the composites. The 3D image of the composite could be obtained by integrating all the cross-sectional 2D images of the sample. The actual dispersion state of the composite could be clearly observed using micro-CT analysis. The G150 composite was considered as a model to scrutinize the dispersibility of the filler in the composite. The uniform dispersion of filler regardless of the filler content in the composite could be observed from the 3D images. The 3D micro-CT tomography images showed the

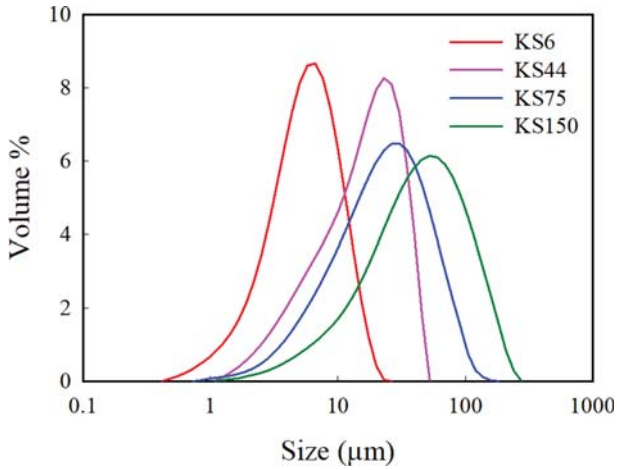

Fig. 2. Particle size distribution of graphite: (a) KS6, (b) KS44, (c) KS75 and (d) KS150.

variations of network formation according to the loading of the filler (Fig. 3). Additionally, cross section SEM microphotographs of G150-filled composites also showed the good distribution of the graphite in paraffin matrix (Fig. S1).

To understand the possible electromagnetic wave attenuation mechanism of the composites, the real part of complex permittivity (ε') and the imaginary part of complex permittivity (ε'') are shown in Fig. 4, and the dielectric loss tangent ($\tan\delta=\varepsilon''/\varepsilon'$) is depicted in Fig. 5. The complex permittivity value was calculated using the

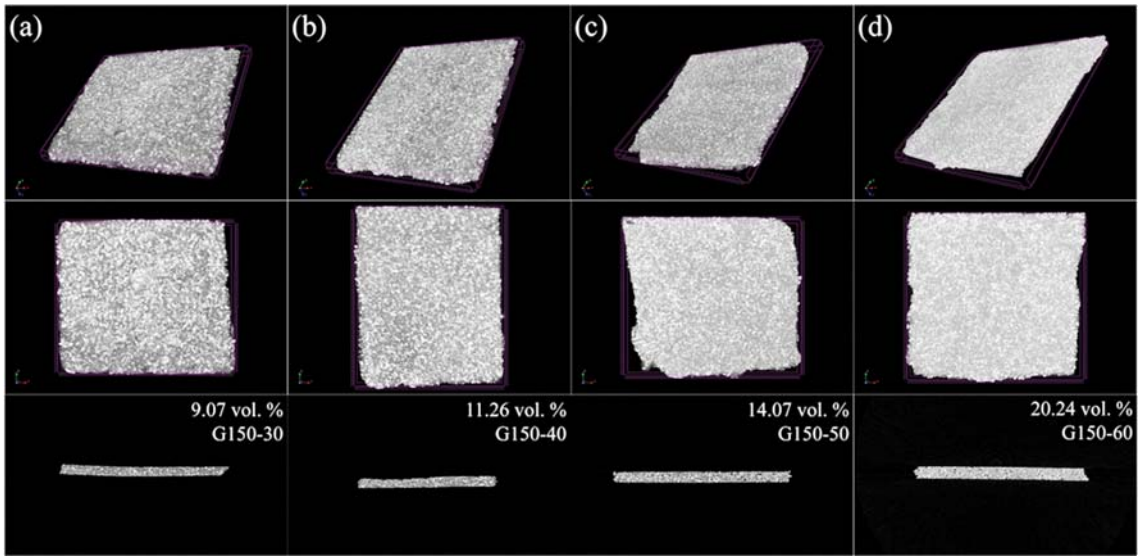

Fig. 3. Micro CT images of G150 composites: (a) G150-30, (b) G150-40, (c) G150-50, and (d) G150-60 (size of specimens: 10.0×10.0×2.0 mm^3).

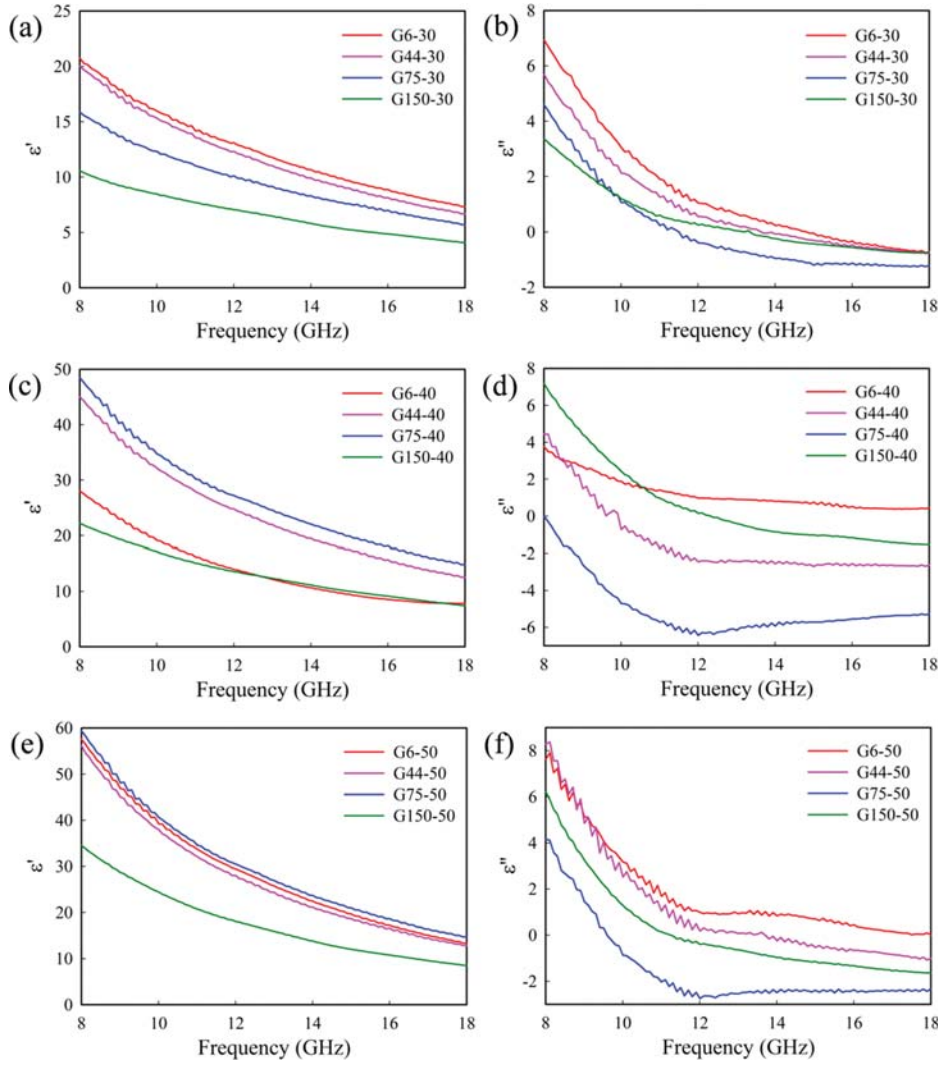

Fig. 4. Complex permittivity of composites filled with graphite of various sizes (a), (b) content 30 wt%, (c), (d) filler content 40 wt% and (e), (f) filler content 50 wt%.

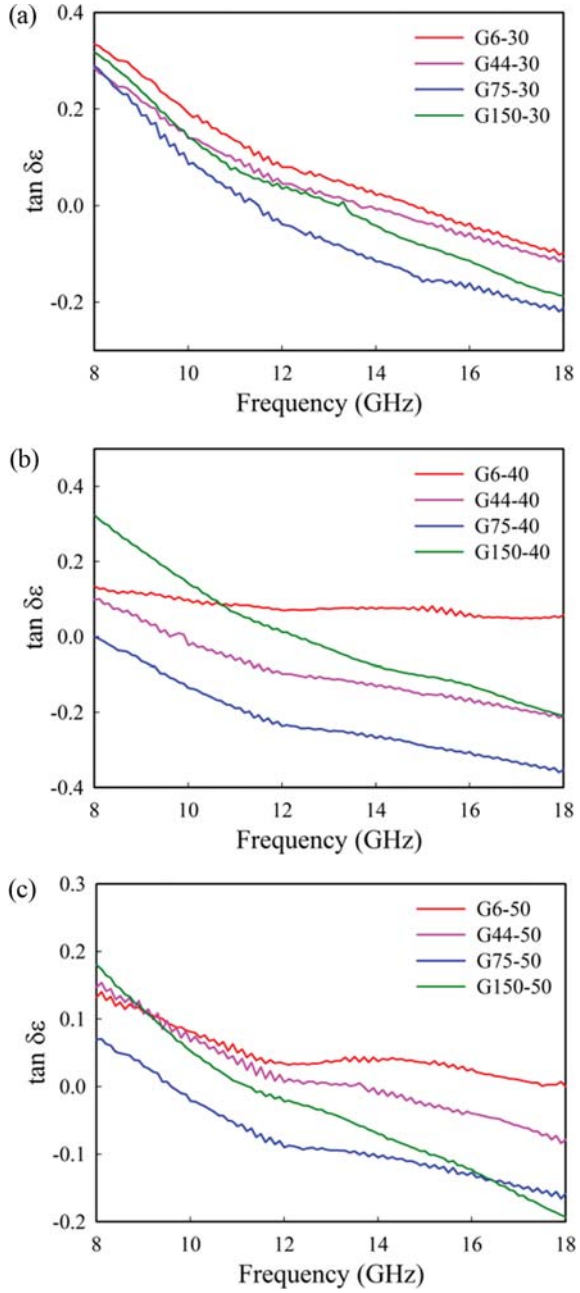

Fig. 5. Dielectric loss of composites filled with graphite of various sizes (a) filler content 30 wt%, (b) filler content 40 wt% and (c) filler content 50 wt%.

Nicolson-Ross-Weir (NRW) method [30-34]. Theoretically, permittivity is the complex form of real and imaginary parts. The real part indicates the relative permittivity (dielectric constant), while the imaginary one is related to the loss of EM wave. The relative permittivity of a material is the ratio of the permittivity of the material to the permittivity of vacuum. The complex permittivity values of graphite and paraffin wax composites are shown in Fig. 4. From the results shown in Fig. 4(a), (c), and (e), we found that the relative permittivity (real part of complex permittivity, ε') of the composites increases with increasing the graphite loading. Increasing the loading of graphite will lead to an increment in "numbers" of dielectric

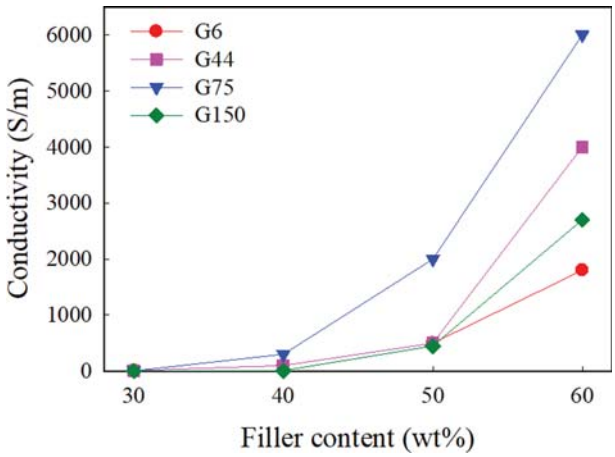

Fig. 6. Conductivity of composites filled with graphite of various sizes in the range of 30-60 wt% filler contents.

polarization of composites; the increased "numbers" of dielectric polarization of composites will result in higher relative permittivity. The imaginary part of complex permittivity was also found to be proportional to the loading of graphite. As mentioned, the imaginary part of complex permittivity represents the loss information of EMI shielding material. The electrical conductivity of composite increases with increasing the loading of graphite. Thus, the imaginary part of complex pemittivity should be proportional to the electrical conductivity of the composite; the correlation between the imaginary part of complex permittivity and electrical conductivity can be proved to be theoretically correct by Eq. (1).

$$\varepsilon'' = \frac{\sigma}{\omega} = \frac{\sigma}{2\pi f} \tag{1}$$

Dielectric loss shown in Fig. 5 was difficult to correlate with the loading of graphite because the real and imaginary parts of permittivity increase simultaneously. In Fig. 6, G75 composite shows the highest electrical conductivity with 30-60 wt% graphite loading, which is consistent with relative permittivity and dielectric loss [35]. G150 composites also exhibit the lowest electrical conductivity up to a loading of 50 wt%. However, the electrical conductivity increases to 27 S/m at 60 wt%, which is higher than that obtained with 60 wt% of G6 composite. By comparing the electrical conductivity values of the composites, we observed that the small-sized filler has a higher electrical conductivity at low loading, but the degree of enhancement of the electrical conductivity is weaker than that of large-sized graphite. These phenomena result from the differences in the ratio of surface area to volume of the graphite. The higher exposed surface at low loading implies the higher probability of effective contact of the filler within the composite. Thus, the small-sized filler displays a better performance than the large-sized one. However, with an increase in the loading, enough contacts of the filler particles within the composite are formed in all cases of the composites. Consequently, the larger-sized graphite demonstrates a smaller contact resistance and a much higher electrical conductivity.

The total SE of the material, SE (T), is calculated by the summation of reflection SE (R) and absorption SE (A) [36]. In a two-port VNA, the SE (R) and SE (A) values can be determined by cal-

Table 1. Summary of electrical conductivity and electromagnetic interference shielding effectiveness (EMI SE) of composites

Sample	Relative permittivity at 8 GHz (dB)	Relative permittivity at 18 GHz (dB)	Conductivity (S/m)
G6-30	20.74	7.35	10
G6-40	27.99	7.83	100
G6-50	57.51	13.37	500
G6-60	-	-	1,800
G44-30	20.02	6.70	10
G44-40	45.01	12.55	100
G44-50	56.15	12.84	500
G44-60	-	-	4,000
G75-30	15.86	5.72	7.0
G75-40	48.47	14.82	300
G75-50	59.34	14.70	2,000
G75-60	-	-	6,000
G150-30	10.56	4.10	1.0
G150-40	22.21	7.48	10
G150-50	34.52	8.59	450
G150-60	-	-	2,700

culating the reflectance (R) and transmittance (T) coefficients, which are correlated with the scattering parameters (S_{11}, S_{12}, S_{21}, S_{22}) as follows:

$$R=|S_{11}|^2=|S_{22}|^2,\ T=|S_{12}|^2=|S_{21}|^2 \quad (2)$$

SE (R) and SE (A) can be defined in terms of scattering parameters as follows:

$$SE(R)=10\log\left(\frac{1}{1-R}\right)=10\log\left(\frac{1}{1-|S_{11}|^2}\right) \quad (3)$$

$$SE(A)=10\log\left(\frac{1-R}{T}\right)=10\log\left(\frac{1-|S_{11}|^2}{|S_{21}|^2}\right) \quad (4)$$

SE (T) can be calculated from Eqs. (3) and (4) as follows:

$$SE(T)=20\log(S_{21}) \quad (5)$$

Table 1 summarizes the correlation between EMI SE performance and electrical conductivity and provides an overview of the relationship between electrical conductivity and EMI SE performance. The tendency of the electrical conductivity and composite content in Table 1 and Fig. 6 shows that the graphite content is G44>=G6> G75> G150 at 30 wt%, and G75> G44>=G6> G150 at 40 and 50 wt%. At 60 wt% of graphite loading, the trend of G75> G44> G150> G6 was confirmed. Thus, it could be concluded that with increasing the loading of graphite, the degree of reinforcement of electrical conductivity of larger-sized graphite (G150 and G75) exhibited faster than that of smaller-sized graphite (G44 and G6). Also, the conductivity was consistent with the tendency of relative permittivity. The calculated EMI SE curves of the graphite composites with various loadings are shown in Fig. 7. The 30 wt% graphite-filled composites shown in Fig. 7(a) demonstrate an overall low SE (T). The SE (R) values do not show substantial differences when the filler content is 30 wt%. However, the SE (A) values exhibit significant differences when the filler size is varied. When the the filler is small, the distance between the fillers is closer than that obtained for the large sized-filler. In case of G150-30, the SE (T) value was less than 10 dB, because a large amount of electromagnetic waves leaked out from the gaps between adjacent fillers. This tendency declines, as the filler content increases. Finally, when the filler content is 50 wt%, the G150-50 composite exhibits an electromagnetic shielding ability of 40 dB or higher. In this aspect, we suggest that large-sized graphite is better than small-sized one. However, the opposite effect can be observed when the size of the graphite is enormous. When the electrical conductivity is approximately 100 S/m or higher, the EMI SE value can exceed 30 dB. To attain an EMI SE performance over 40 dB, the electrical conductivity must be higher than 500 S/m.

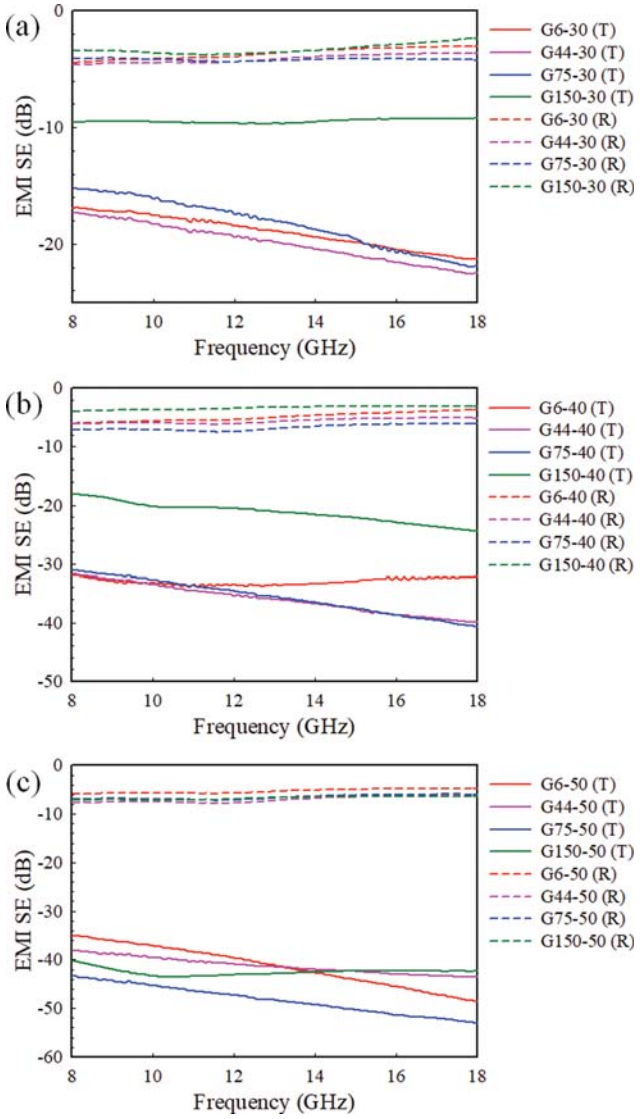

Fig. 7. EMI SE of composites filled with graphite of various sizes: (a) 30 wt% graphite, (b) 40 wt% graphite and (c) 50 wt% graphite.

From Table 1, G75-50 composite has the most superior EMI SE performance of 53.0 dB at 18 GHz and an electrical conductivity of 2,000 S/m. Again, Fig. 4 shows the high relative permittivity and

low imaginary part of permittivity of the G75 composite. Additionally, G75 composites demonstrate the lowest dielectric loss as seen in Fig. 5. From the internal topology of the composites using micro-CT, the geometric characteristics of fillers, namely the spacing between the fillers, exerts a profound effect on both electrical conductivity and EMI SE performance. This finding is consistent with the trend of the EMI SE performance of G150 composites listed in Table 1. The type and content of filler required for a specific EMI SE performance can be determined using the values listed in Table 1. To achieve an EMI SE performance of 30 dB, the loading amount must not be less than 40 wt% in case of KS6, KS44, and KS75. To achieve a performance of 40 dB, the content of graphite must be increased to half of that of the composite (50 wt%).

CONCLUSIONS

Graphite has a high relative permittivity and electrical conductivity due to its low aspect ratio and graphene-based structure. According to its structural features, the effects of sizes of graphite in EMI shielding performance were examined by changing the sizes and loadings of graphite in the composites. Because of the similar intrinsic attractive force, London dispersion force, between graphite and paraffin matrix, the dispersion degree of the graphite within the composite is independent of the graphite size. By adopting 3D micro-CT analysis, the geometric characteristics of graphites and the spacing between graphites were investigated. According to the 3D micro-CT results, the spacing between graphite becomes narrower as the loading amount increases. The complex permittivity and dielectric loss were also calculated by substituting the S parameter and the phase difference obtained from the 2-ports VNA into the NRW method. Among composites, G75 composites showed the highest relative permittivity and excellent electrical conductivity; consequently, it exhibited the best EMI SE performance. Small-sized fillers had a relatively high electrical and EMI SE performance at low loading amounts; however, their performance was worse than that of G75 at higher loading. Moreover, we discovered that the large-sized filler is suitable only for high loading circumstances. According to the results, it is evident that selecting the appropriate size and loading of the graphite is critical in fabricating the desired EMI shielding materials.

ACKNOWLEDGEMENTS

This work was supported by the Ministry of Trade, Industry & Energy (MOTIE, Korea) under the Industrial Technology Innovation Program (grant No.: 10052976).

SUPPORTING INFORMATION

Additional information as noted in the text. This information is available via the Internet at http://www.springer.com/chemistry/journal/11814.

REFERENCES

1. Z. Dang, T. Zhou, S. Yao, J. Yuan, J. Zha, H. Song, J. Li, Q. Chen, W. Yang and J. Bai, *Adv. Mater.*, **21**, 2077 (2009).
2. P. C. P. Watts, W. Hsu, A. Barnes and B. Chambers, *Adv. Mater.*, **15**, 600 (2003).
3. Z. Chen, C. Xu, C. Ma, W. Ren and H. Cheng, *Adv. Mater.*, **25**, 1296 (2013).
4. K. S. Novoselov, A. K. Geim, S. V. Morozov, D. Jiang, Y. Zhang, S. V. Dubonos, I. V. Grigorieva and A. A. Firsov, *Science*, **306**, 666 (2004).
5. D. D. L. Chung, *Carbon*, **39**, 279 (2001).
6. N. F. Colaneri and L. W. Shacklette, *IEEE Trans. Instrum. Meas.*, **41**, 291 (1992).
7. S. Geetha, K. K. S. Kumar, C. R. K. Rao, M. Vijayan and D. C. Trivedi, *J. Appl. Polym. Sci.*, **112**, 2073 (2009).
8. C. W. Chu, J. Ouyang, J. Tseng and Y. Yang, *Adv. Mater.*, **17**, 1440 (2005).
9. C. Xiang, Y. Pan, X. Liu, X. Sun, X. Shi and J. Guo, *Appl. Phys. Lett.*, **87**, 123103 (2005).
10. J. Joo and A. Epstein, *Appl. Phys. Lett.*, **65**, 2278 (1994).
11. J. Joo and C. Y. Lee, *J. Appl. Phys.*, **88**, 513 (2000).
12. Z. Liu, G. Bai, Y. Huang, Y. Ma, F. Du, F. Li, T. Guo and Y. Chen, *Carbon*, **45**, 821 (2007).
13. G. Wang, Z. Gao, S. Tang, C. Chen, F. Duan, S. Zhao, S. Lin, Y. Feng, L. Zhou and Y. Qin, *ACS Nano*, **6**, 11009 (2012).
14. Z. Liu, G. Bai, Y. Huang, Y. Huang, F. Li, Y. Ma, T. Guo, X. He, X. Lin, H. Gao and Y. Chen, *J. Phys. Chem. C.*, **111**, 13696 (2007).
15. Y. Wang, L. Huang, Y. Liu, D. Wei, H. Zhang, H. Kajiura and Y. Li, *Nano Res.*, **2**, 865 (2009).
16. Y. Wang, M. Jaiswal, M. Lin, S. Saha, B. Ozyilmaz and K. P. Loh, *ACS Nano*, **6**, 1018 (2012).
17. Y. Yang, M. C. Gupta, K. L. Dudley and R. W. Lawrence, *Nano Lett.*, **5**, 2131 (2005).
18. S. K. Hong, K. Y. Kim, T. Y. Kim, J. H. Kim, S. W. Park, J. H. Kim and B. J. Cho, *Nanotechnology*, **23**, 455704 (2012).
19. D. Yan, H. Pang, B. Li, R. Vajtai, L. Xu, P. Ren, J. Wang and Z. Li, *Adv. Funct. Mater.*, **25**, 559 (2015).
20. Q. Song, F. Ye, X. Yin, W. Li, H. Li, Y. Liu, K. Li, K. Xie, X. Li, Q. Fu, L. Cheng, L. Zhang and B. Wei, *Adv. Mater.*, **29**, 1701583 (2017).
21. Y. Zhan, J. Wang, K. Zhang, Y. Li, Y. Meng, N. Yan, W. Wei, F. Peng and H. Xia, *Chem. Eng. J.*, **44**, 184 (2018).
22. L. C. Jia, D. X. Yan, Y. Yang, D. Zhou, C. H. Cui, E. Bianco, J. Lou, R. Vajtai, B. Li, P. M. Ajayan and Z. M. Li, *Adv. Mater. Technol.*, **2**, 1700078 (2017).
23. M. Verma, P. Verma, S. K. Dhawan and V. Choudhary, *RSC Adv.*, **5**, 97349 (2015).
24. S. Yang, W. Li, S. Bai, and Q. Wang, *J. Mater. Chem. C*, **6**, 11209 (2018).
25. G. D. Bellis, A. Tamburrano, A. Dinescu, M. L. Santarelli and M. S. Sarto, *Carbon*, **49**, 4291 (2011).
26. T. A. Ezquerra, M. Kulescza, C. S. Cruz and F. J. Baltá-Calleja, *Adv. Mater.*, **2**, 597 (1990).
27. Q. Liu, B. Cao, C. Feng, W. Zhang, S. Zhu and D. Zhang, *Compos. Sci. Technol.*, **72**, 1632 (2012).
28. G. Behnam and N. Ghalichechian, *iWAT*, 48 (2016).
29. Z. Han and A. Fina, *Prog. Polym. Sci.*, **36**, 914 (2011).
30. V. R. Tuz, D. V. Novitsky, P. L. Mladyonov, S. L. Prosvirnin and A. V. Novitskyet, *JOSA B*, **31**, 2095 (2014).
31. X. Chen, T. M. Grzegorczyk, B. Wu, J. Pacheco and J. A. Kong, *Phys.*

Rev. E, **70**, 016608 (2004).
32. A. Alù, A. D. Yaghjian, R. A. Shore and M. G. Silveirinha, *Phys. Rev. B*, **84**, 054305 (2011).
33. A. Nicolson and G. Ross, *IEEE Trans. Instrum. Meas.*, **19**, 377 (1970).
34. W. B. Weir, *Proc IEEE*, **62**, 33 (1974).
35. J. Yu, X. Huang, C. Wu and P. Jiang, *IEEE Trans. Dielectr. Electr. Insul.*, **18**, 478 (2011).
36. J. Thomassin, C. Jerome, T. Pardoen, C. Bailly, I. Huynen and C. Detrembleur, *Mater. Sci. Eng. R. Rep.*, **74**, 211 (2013).

Supporting Information

Filler size effect in graphite/paraffine wax composite on electromagnetic interference shielding performance

Sosan Hwang, Chae Lin Kim, Yongha Kim, Min Gyu Song, Jaewon Lee, Sung-Hyeon Baeck, Sang Eun Shim†, and Yingjie Qian†

Department of Chemical Engineering, Inha University, 100 Inha-ro, Michuhol-gu, Incheon 22212, Korea
(*Received 13 November 2019 • Revised 29 February 2020 • Accepted 24 March 2020*)

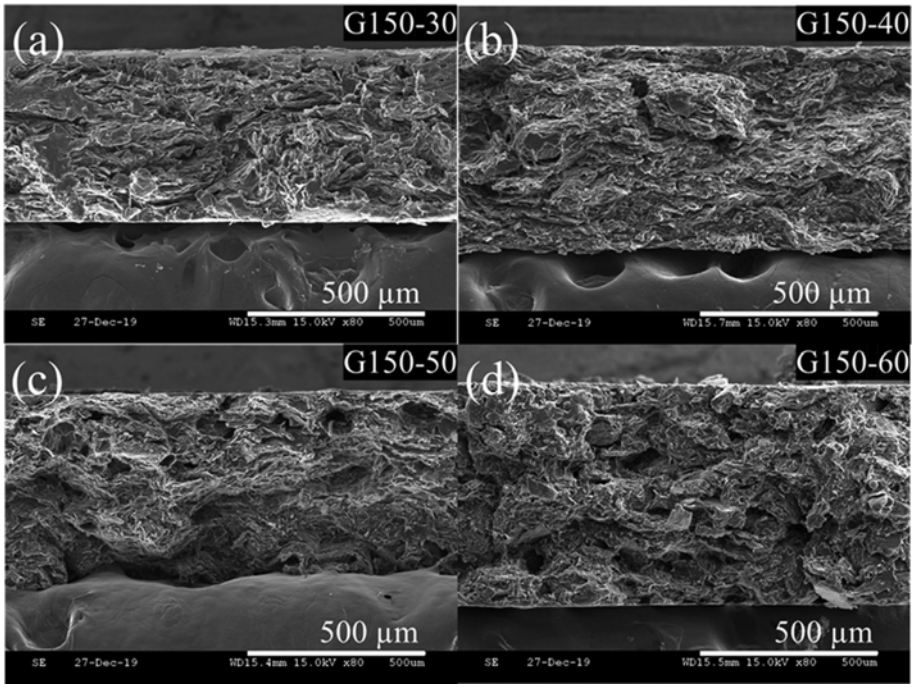

Fig. S1. Cross section SEM microphotographs of G150-filled composites with different graphite loadings.